LETTER

doi:10.1038/nature09971

Substrate-modulated gating dynamics in a Na^+-coupled neurotransmitter transporter homologue

Yongfang Zhao[1,2,4]*, Daniel S. Terry[5]*, Lei Shi[5,6]*, Matthias Quick[1,2,4], Harel Weinstein[5,6], Scott C. Blanchard[5] & Jonathan A. Javitch[1,2,3,4]

Neurotransmitter/Na^+ symporters (NSSs) terminate neuronal signalling by recapturing neurotransmitter released into the synapse in a co-transport (symport) mechanism driven by the Na^+ electrochemical gradient[1–6]. NSSs for dopamine, noradrenaline and serotonin are targeted by the psychostimulants cocaine and amphetamine[1], as well as by antidepressants[7]. The crystal structure of LeuT, a prokaryotic NSS homologue, revealed an occluded conformation in which a leucine (Leu) and two Na^+ are bound deep within the protein[8]. This structure has been the basis for extensive structural and computational exploration of the functional mechanisms of proteins with a LeuT-like fold[9–22]. Subsequently, an 'outward-open' conformation was determined in the presence of the inhibitor tryptophan[23], and the Na^+-dependent formation of a dynamic outward-facing intermediate was identified using electron paramagnetic resonance spectroscopy[24]. In addition, single-molecule fluorescence resonance energy transfer imaging has been used to reveal reversible transitions to an inward-open LeuT conformation, which involve the movement of transmembrane helix TM1a away from the transmembrane helical bundle[22]. We investigated how substrate binding is coupled to structural transitions in LeuT during Na^+-coupled transport. Here we report a process whereby substrate binding from the extracellular side of LeuT facilitates intracellular gate opening and substrate release at the intracellular face of the protein. In the presence of alanine, a substrate that is transported ~10-fold faster than leucine[15,25], we observed alanine-induced dynamics in the intracellular gate region of LeuT that directly correlate with transport efficiency. Collectively, our data reveal functionally relevant and previously hidden aspects of the NSS transport mechanism that emphasize the functional importance of a second substrate (S2) binding site within the extracellular vestibule[15,20]. Substrate binding in this S2 site appears to act cooperatively with the primary substrate (S1) binding site to control intracellular gating more than 30 Å away, in a manner that allows the Na^+ gradient to power the transport mechanism.

The experiments were performed on LeuT engineered to contain a 15-amino-acid, carboxy-terminal biotinylation domain[26] and site-specifically labelled with the fluorophores Cy3 and Cy5 maleimide at residue position 7, after replacing the native His residue with Cys (H7C) in the amino-terminal loop close to TM1, and at position 86 (R86C) in intracellular loop (IL) 1 (Methods). Direct observations of conformational processes within the intracellular gate region of LeuT (Supplementary Fig. 1) were made using a wide field imaging strategy employing prism-based total internal reflection (Methods, Fig. 1a). As described[22], fluorescence resonance energy transfer (FRET) imaging of LeuT revealed two readily distinguished states (FRET efficiency ~0.51 and ~0.75) in the presence of 200 mM K^+ and the nominal absence of Na^+ (Fig. 1b), consistent with the existence of two distinct conformations of the intracellular gate that differ by ~13 Å in the distance separating the fluorophore pair.

In experiments imaging LeuT dynamics with increasing Na^+ concentrations, Hidden Markov Modelling revealed that the distribution of low- and high-FRET conformations of LeuT was altered by Na^+ with an effector concentration for half-maximum response (EC_{50}) of 10.9 mM (Fig. 1b, c), consistent with the EC_{50} for Na^+-dependent stimulation of substrate binding and transport[15]. Na^+ decreased the overall frequency of transitions (Fig. 1d, e) through the preferential stabilization (~7-fold) of the inward-closed state. During the direct imaging of individual LeuT molecules (Fig. 1f), slow, spontaneous transitions between open and closed states, initially observed in 200 mM K^+, were dramatically decreased on exchange into Na^+-containing buffer, leading to the preferential stabilization of the inward-closed state.

Reasoning that substrate-induced intracellular gating might be observed best under conditions mimicking the relatively low intracellular Na^+, we performed experiments at Na^+ concentrations sufficient for Leu binding but below the EC_{50} of Na^+. However, even at 2 mM Na^+, Leu shifted the population towards the closed intracellular gate conformation (Supplementary Fig. 2a, b) through a ~3.5-fold stabilization of this state (Supplementary Fig. 2c). These effects, which result in a global decrease in transition frequency (Supplementary Fig. 2d), were recapitulated at the level of individual LeuT molecules (Supplementary Fig. 2e). Thus, while unambiguously demonstrating binding of both Na^+ and Leu to LeuT, these results corroborate our earlier finding that Leu binding has the net effect of diminishing the likelihood of intracellular gate opening. One possible explanation for these observations is that Leu's high affinity for the transporter[15] makes it a poor substrate for transport, which in our measurements is manifested in the greatly extended lifetime of the closed state. To test this hypothesis, intracellular gate dynamics were assessed in the presence of the more efficiently transported substrate Ala.

In stark contrast to Leu, under otherwise identical conditions, increasing Ala concentrations did not shift the FRET distribution towards the closed state (Fig. 2a, b). Instead, a strong, Ala-concentration-dependent enhancement of transition rates was observed. In 2 mM Na^+, Ala enhanced the transition rates between inward-open and inward-closed states by as much as ~4-fold (Fig. 2c, d). This result was directly confirmed at the scale of individual molecules on exchange into Ala-containing buffer (Fig. 2e). Similar enhancements in transition frequency were also

[1]Center for Molecular Recognition, Columbia University College of Physicians and Surgeons, 630 West 168th Street, New York, New York 10032, USA. [2]Department of Psychiatry, Columbia University College of Physicians and Surgeons, 630 West 168th Street, New York, New York 10032, USA. [3]Department of Pharmacology, Columbia University College of Physicians and Surgeons, 630 West 168th Street, New York, New York 10032, USA. [4]Division of Molecular Therapeutics, New York State Psychiatric Institute, 1051 Riverside Drive, New York, New York 10032, USA. [5]Department of Physiology and Biophysics, Weill Medical College of Cornell University, 1300 York Avenue, New York, New York 10021, USA. [6]HRH Prince Alwaleed Bin Talal Bin Abdulaziz Alsaud Institute for Computational Biomedicine, Weill Cornell Medical College, Cornell University, 1300 York Avenue, New York, New York 10021, USA.
*These authors contributed equally to this work.

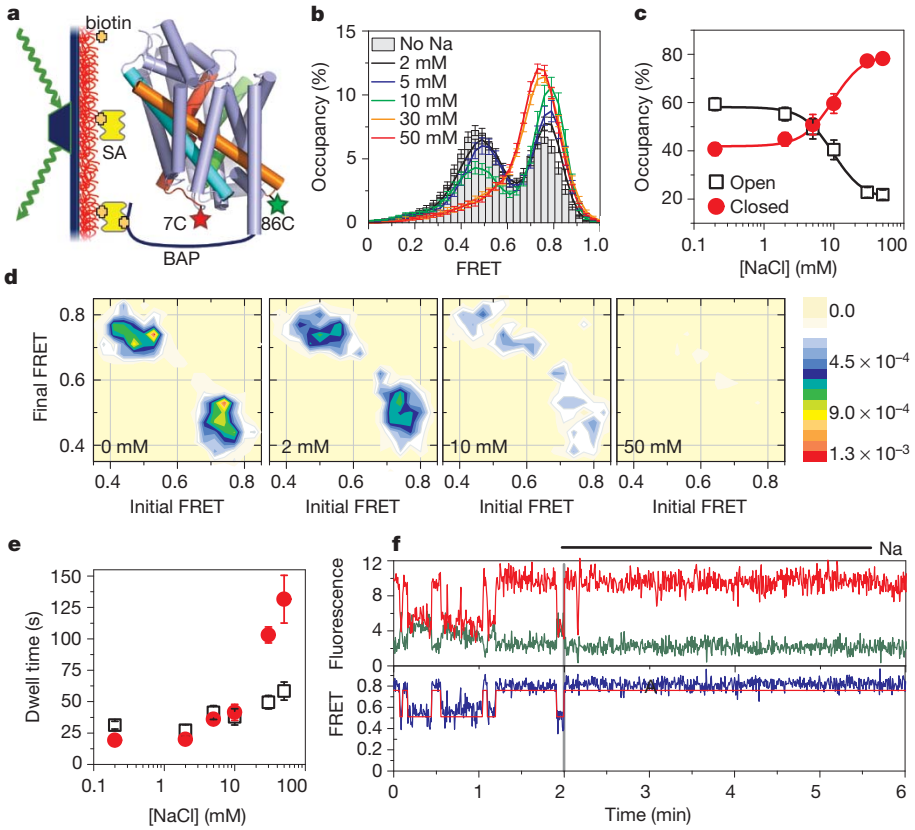

Figure 1 | Effect of Na^+ on LeuT dynamics. **a**, Experimental set-up: H7C/R86C-LeuT labelled with Cy3 and Cy5 (stars) was immobilized via a biotin acceptor peptide (BAP) on a passivated glass surface and illuminated using total internal reflection. FRET traces (>110 per condition) were collected with varying concentrations of Na^+ (160-ms time resolution for all, except 30–50 mM with 400 ms). **b**, Histograms of FRET traces, filtered to remove fluorophore dark states. **c**, Fraction of time in the lower-FRET open state (black open squares) and the high-FRET closed state (red filled circles). **d**, Transition density plot: average FRET values before (*x* axis) and after (*y* axis) each transition were plotted as a two-dimensional chart in transitions per second (scale at right; Na^+ concentrations are indicated). **e**, Average dwell times in each state. **f**, Representative traces (donor in green, acceptor in red, FRET in blue, and predicted state sequence (idealization) in red), where the solution was exchanged at 2 min from K^+ to Na^+ (200 mM). Error bars, s.d. of ≥100 bootstrap samples.

observed for H7C/T515C-LeuT (Supplementary Fig. 3). In accordance with such effects, which required both Na^+ and Ala, the lifetimes of the inward-open or inward-closed FRET states were not significantly affected by Ala alone (in the nominal absence of Na^+); at 250 μM Ala, the transition frequency increased in a Na^+-concentration-dependent fashion (Supplementary Fig. 4).

Using transition state theory (Methods), we found that the intracellular open and closed FRET states of LeuT were separated by a large activation barrier ($\Delta G^{\ddagger} \approx 80\ kJ\ mol^{-1}$). Ala does not alter the relative occupancies of open and closed states, but instead lowers the activation barrier for both open-to-closed and closed-to-open transitions by approximately $3\ kJ\ mol^{-1}$ (about the energy of a hydrogen bond). By contrast, Leu raised the activation barrier for the closed-to-open transition by as much as $4\ kJ\ mol^{-1}$, apparently through ground-state stabilization of the closed state.

Hypothesizing that the observed dynamics reflect Ala's acceleration of the opening-closing cycles of the intracellular gate required for the transport mechanism, we performed experiments in the presence of the transport inhibitor clomipramine (CMI), a tricyclic antidepressant that is known to bind in an extracellular vestibule above the Na^+ and S1 binding sites[25,27,28]. Many of the residues shown to interact with antidepressants in these structures are also part of the S2 site[25,27]. As substrate binding in the S2 site is thought to allosterically trigger intracellular release of Na^+ and substrate from the S1 site[15] (also see Supplementary Fig. 1), CMI should block Ala-induced intracellular gating dynamics. Indeed, in the presence of both Na^+ and Ala, CMI essentially eliminated intracellular gate opening, stabilizing LeuT in a high-FRET, inward-closed conformation (Supplementary Fig. 5a–c). This observation is consistent with CMI competitively blocking substrate binding to the S2 site[15], thereby preventing Ala-induced opening and closing of the intracellular gate, and inhibiting transport. This result was again confirmed by direct imaging of individual LeuT molecules in Na^+ and Ala-containing buffer on addition of CMI (Fig. 2f). The detergent n-octyl-β-D-glucopyranoside also inhibited intracellular gating dynamics (Supplementary Fig. 5a–c), consistent with its capacity to disrupt the Na^+-coupled transport mechanism[20] by competing with substrate binding to the S2 site[20,23].

To probe whether Ala binding to the S1 and/or S2 site(s) was responsible for lowering the activation barrier for intracellular gating dynamics, single-molecule FRET experiments were performed in the background of either an F253A or L400S mutation within the S1 or S2 site, respectively (Fig. 3a, Supplementary Fig. 1). These mutations disrupt substrate binding to LeuT, decreasing the stoichiometry of substrate:LeuT binding under saturating conditions from 2:1 in wild-type LeuT, to 1:1 in both mutants (Fig. 4a). Mutation of F253 blocks substrate binding to the S1 site and also abrogates transport (Fig. 4a, b; Supplementary Fig. 6), while having little or no effect on Na^+ binding (Supplementary Table 1). Despite evidence that Ala bound to the S2 site in the context of the F253A mutation (Fig. 4a), Ala failed to increase intracellular gating dynamics of the mutant protein (Fig. 4c). Similarly, despite evidence of Ala binding to the S1 site (Fig. 4a), no increase in intracellular gating dynamics was observed when the S2 site was disrupted by the L400S mutation (Fig. 4c). These findings support the notion that substrate occupancy in the S2 site is critical for the allosteric mechanism that controls intracellular gate opening and the release of substrate from the S1

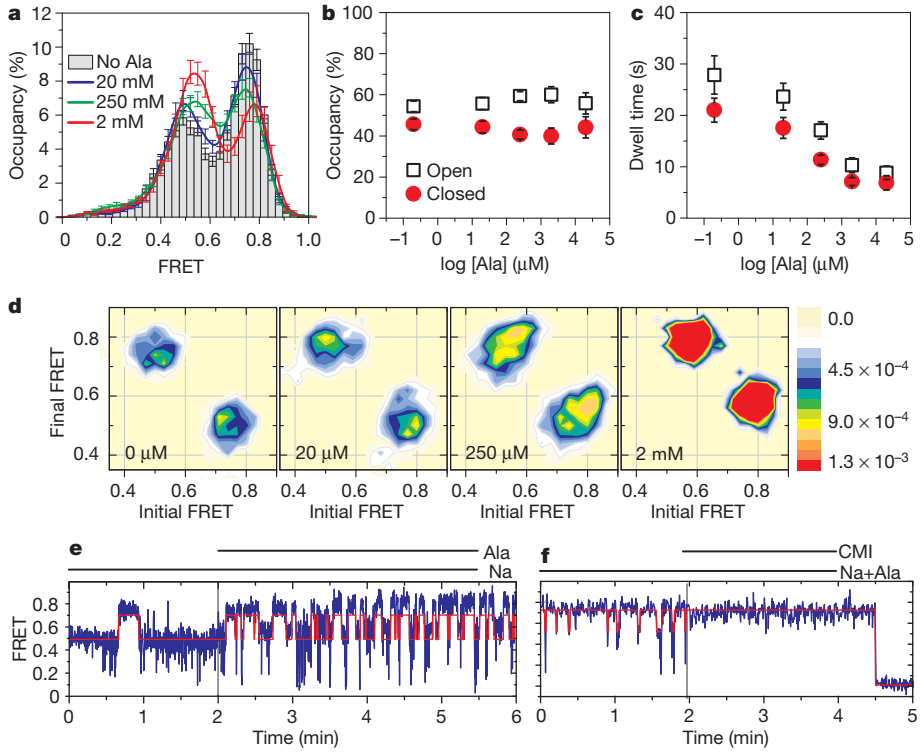

Figure 2 | Effect of alanine on LeuT dynamics. Single-molecule FRET traces (>90 per condition) were collected at 160-ms time resolution with 2 mM Na^+ and varying concentrations of Ala. **a**, Histograms of FRET data from each condition. Hidden Markov Modelling analysis revealed the fraction of time (**b**) and average dwell times (**c**) in the lower-FRET open state (black open squares) and the high-FRET closed state (red filled circles). **d**, Transition density plots as in Fig. 1d (Ala concentrations are indicated). **e**, **f**, Representative FRET traces (blue) with idealization (red) from experiments where solution was exchanged at 2 min: **e**, 2 mM Na^+, adding 250 μM Ala; **f**, 2 mM Na^+ and 250 μM Ala, adding the inhibitor clomipramine (CMI; 0.5 mM). Error bars, s.d. of ≥100 bootstrap samples.

site[15], and demonstrate that substrate binding to both the S1 and S2 sites is necessary to trigger intracellular gating.

In order to probe whether Ala binding to the S1 and S2 sites is also sufficient to promote intracellular gating and transport, experiments were performed in the presence of Li^+ in place of Na^+. In the presence of saturating Li^+ concentrations (>150 mM), we found that Ala binds LeuT with a 2:1 stoichiometry consistent with both S1 and S2 site occupancy (Fig. 4a). Li^+, like Na^+, stabilized the inward-closed state (Supplementary Fig. 7), but, in the presence of Li^+, Ala failed to accelerate intracellular gating dynamics and no substrate transport was observed (Fig. 4c). Instead, the inward-closed conformation of LeuT was modestly stabilized in the presence of Ala (~2-fold reduction in the rate of gate opening, $k_{closed\text{-}open}$) (Fig. 4c). These data demonstrate that Ala binding to the S1 and S2 sites in the presence of Li^+ does not lower the activation barrier to intracellular gating as observed in the presence of Na^+.

Prompted by these experimental observations, computational studies were performed to investigate how both Na^+ and Li^+ can support substrate binding to LeuT, whereas only Na^+ leads to substrate-induced dynamics of the intracellular gate and to transport. These studies also

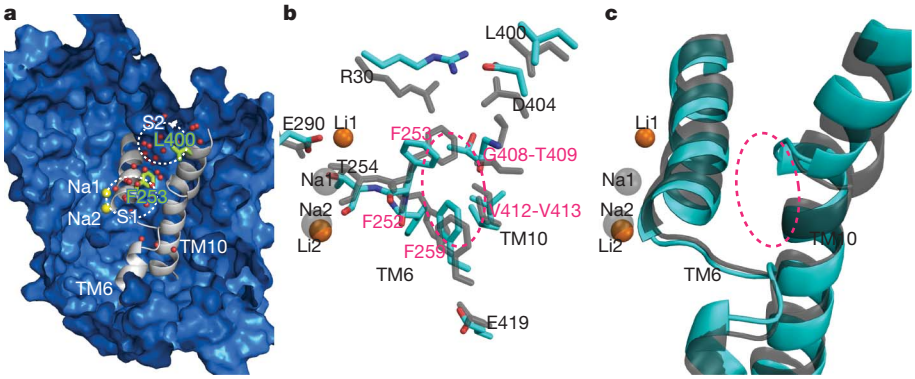

Figure 3 | The configuration of TM6–TM10 interactions induced by Na^+ binding cannot be matched by Li^+ binding. **a**, Representative snapshot taken from the Na-only simulation, showing water molecules (red spheres) occupying the S1 and S2 sites (white dotted ellipses). Residues L400 in the S2 site and F253 in the S1 site, which were mutated to affect substrate binding, are shown as light green sticks. **b**, The different effects that Li^+ and Na^+ binding have on the interacting residues of TM6 and TM10. The TM6/TM10 interface is indicated by the dashed ellipse in magenta. **c**, The bulge around G408 in TM10, which is present only when Na^+ is bound but not when Li^+ replaces it. In **b** and **c**, side chains and backbones coloured according to atom types are from the Li-only conformation, while those from the Na-only conformation are rendered in grey.

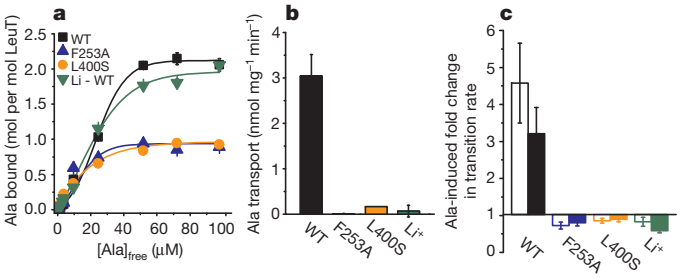

Figure 4 | Effect of S1 and S2 site mutations and of Li^+ on activity and dynamics. **a**, Binding of ^{3}H-Ala in buffer containing 50 mM Na^+ was measured for wild-type (WT, black squares), F253A (blue triangles) and L400S (orange circles) LeuT, and for wild-type LeuT with 150 mM Li^+ (green inverted triangles). **b**, ^{3}H-Ala uptake with 100 mM Na^+ was measured for WT (black), F253A (blue) and L400S (orange) LeuT or with 150 mM Li^+ for WT LeuT (green). Error bars in **a** and **b**, s.e.m. of triplicate determinations. **c**, The fold change in the rate of transitioning from the open state to the closed state (open bars) and from the closed state to the open state (filled bars) induced by 250 μM Ala in 10 mM Na^+ or for WT in 40 mM Li^+ (>280 traces and 800 transitions per condition). Error bars in **c**, s.d. of ≥100 bootstrap samples.

served to identify both local changes produced in the region of the ion binding sites and critical elements in the allosteric pathway linking the substrate binding sites and the intracellular gate region. Comparative analysis of separate molecular dynamics (MD) simulations of LeuT, performed with either Na^+ or Li^+ occupying the established Na^+ binding sites and in the absence of amino acid substrate (termed Na-only[24] and Li-only, respectively) revealed significant differences in TM–TM interactions (Fig. 3b, c), which are described in detail in Supplementary Information. The Na1/Li1 binding site and its neighbouring interaction network, which are crucial for the proper propagation of the allosteric effects from the S2 to S1 site (see Supplementary Information for details) and onward to the intracellular side to open the transport pathway, are sensitive to the unique combination of the ionic radius of the Na^+ cation and the charge redistribution it causes. The structural consequences of the ion-specific effects appear to be propagated through the cluster of aromatic residues at the heart of the S1 binding site, and result in different configurations of the bulge in the middle of TM10 (Fig. 3, Supplementary Fig. 8).

The positions of the structural elements involved in this propagation mechanism make them critical for transmitting conformational changes deeper into the TM bundle towards the intracellular end of the transporter (Fig. 3b, c). Such changes include local alterations in the vicinity of E419, a residue known from the crystal structure to interact with E62 in TM2, with the backbone of the unwound portion of TM6 (proximal to F259 of the aromatic cluster and the S1 binding site), and two water molecules[29]. Reconfiguration of this region, including residue T418, on simulated inward movement of the substrate[15] was previously shown to enable the penetration of water from the intracellular side of LeuT as a result of an opening at IL1[15]. The resulting dissociation of IL1 from interactions with R5 and D369 and the destabilization of the network of intracellular interactions detected in the simulations (Supplementary Fig. 9) is associated with the observed outward movement of TM1a[22] that is essential for the simulated release of substrate to the intracellular side.

Owing to the different effects of Li^+ and Na^+, Ala binding in both the S1 and S2 sites in the presence of Li^+ would not engender the ordered series of local conformational rearrangements expected in the presence of Na^+. These rearrangements originate in the S2 site and need to be propagated as described above through changes in the Na1 and S1 sites to enable water penetration from the cytoplasmic side of LeuT and the outward movement of TM1a. Their absence when Li^+ substitutes for Na^+ would explain why substrate-induced acceleration of gating dynamics was not observed experimentally.

Na^+ binding, which stabilizes the inward-closed state, does not hasten gate closure but, instead, slightly stabilizes the inward-open state as well, by raising the energy barrier to the conformational transition. In contrast, Ala binding to LeuT in the presence of Na^+ shortens not only the inward-closed, but also the inward-open, lifetime (Fig. 2). Thus, bound Ala facilitates both the opening of the intracellular gate and its subsequent closure by reducing the activation barrier for such conformational transitions. One possible explanation for this observation is that binding of substrate in the S2 site triggers the opening of the intracellular gate and release of the S1 substrate to the cytoplasm. In the absence of S1 substrate and bound Na^+, substrate in the S2 site may then facilitate intracellular gate closure. It is tempting to speculate that the S2 substrate, in the presence of extracellular Na^+, may move to the S1 site with high efficiency owing to its very high local concentration, thereby facilitating a subsequent transport cycle.

Collectively, our findings support the notion that the observed movements of TM1a and its environment are associated with LeuT intracellular gating[22] in a manner that is directly linked to the Na^+-driven transport mechanism. Thus, results obtained with the slowly transported substrate, Leu, and the relatively rapidly transported substrate, Ala, establish a relationship between the rates of intracellular gating and substrate transport. The role of substrate binding at the S2 site in the process of allostery and molecular recognition is further highlighted by the comparative effects of CMI and Ala binding to this site in the presence of Na^+. The former stabilizes a closed intracellular gate conformation, whereas the latter substantially lowers the activation barrier to gate opening and thereby allows the energy of the Na^+ gradient to drive the transport mechanism.

After the present manuscript had been submitted, a report[30] was published that concluded, on the basis of a variety of binding measurements, that LeuT has only a single high-affinity substrate site. In contrast, our substrate binding measurements clearly show a stoichiometry of 2:1, consistent with high affinity binding to both the S1 and S2 sites[20]. Half of this binding is lost in the S2-site mutant that also exhibits a loss of substrate-induced single-molecule dynamics and transport (Fig. 4). Although the loss of substrate-induced dynamics and transport in the S2-site mutant could conceivably be explained solely by a long-range allosteric effect of the mutation, all our data to date are most consistent with a two-substrate-site model in which the absence of either S1 or S2 substrate binding results in a profound attenuation of transporter dynamics and function. We are currently uncovering the reasons for the discrepancy between the data of ref. 30 and our own data, and will report our findings in due course.

METHODS SUMMARY

LeuT mutants were expressed in *Escherichia coli*, purified, and labelled on targeted engineered cysteines with Cy3 and Cy5 maleimide. The functional properties of the labelled constructs were determined by measuring Leu binding and Na^+ by scintillation proximity assay, and Ala transport was measured after reconstitution of the protein into proteoliposomes. Purified, labelled protein was immobilized onto a passivated glass surface via a streptavidin-biotin linkage (shown schematically in Fig. 1a). Fluorescence data were acquired using a prism-based total internal reflection (TIR) microscope. FRET efficiency was calculated and analysis of fluorescence and FRET traces was achieved using semi-automated analysis software developed for this application. The single-molecule traces were analysed for LeuT in the presence and absence of the substrates Na^+, Leu and Ala, and on addition of the transport inhibitors CMI and n-octyl-β-D-glucopyranoside, and in response to mutations of the S1 and S2 binding sites. MD simulations were carried out with the protein immersed in an all-atom model of the membrane, solvated with water molecules, ions and ligands. Long equilibrations (totalling >2 μs) were run to assess conformational changes, with more than one MD trajectory collected for every configuration mentioned.

Full Methods and any associated references are available in the online version of the paper at www.nature.com/nature.

Received 12 August 2010; accepted 25 February 2011.
Published online 24 April 2011.

1. Amara, S. G. & Sonders, M. S. Neurotransmitter transporters as molecular targets for addictive drugs. *Drug Alcohol Depend.* **51,** 87–96 (1998).

2. Rudnick, G. *Mechanisms of Biogenic Amine Neurotransmitter Transporters* 2nd edn (Humana, 2002).
3. Sonders, M. S., Quick, M. & Javitch, J. A. How did the neurotransmitter cross the bilayer? A closer view. *Curr. Opin. Neurobiol.* **15,** 296–304 (2005).
4. Gu, H., Wall, S. C. & Rudnick, G. Stable expression of biogenic amine transporters reveals differences in inhibitor sensitivity, kinetics, and ion dependence. *J. Biol. Chem.* **269,** 7124–7130 (1994).
5. Torres, G. E., Gainetdinov, R. R. & Caron, M. G. Plasma membrane monoamine transporters: structure, regulation and function. *Nature Rev. Neurosci.* **4,** 13–25 (2003).
6. Krause, S. & Schwarz, W. Identification and selective inhibition of the channel mode of the neuronal GABA transporter 1. *Mol. Pharmacol.* **68,** 1728–1735 (2005).
7. Iversen, L. Neurotransmitter transporters and their impact on the development of psychopharmacology. *Br. J. Pharmacol.* **147** (Suppl 1), S82–S88 (2006).
8. Yamashita, A. *et al.* Crystal structure of a bacterial homologue of Na^+/Cl^--dependent neurotransmitter transporters. *Nature* **437,** 215–223 (2005).
9. Beuming, T., Shi, L., Javitch, J. A. & Weinstein, H. A comprehensive structure-based alignment of prokaryotic and eukaryotic neurotransmitter/Na^+ symporters (NSS) aids in the use of the LeuT structure to probe NSS structure and function. *Mol. Pharmacol.* **70,** 1630–1642 (2006).
10. Quick, M. *et al.* State-dependent conformations of the translocation pathway in the tyrosine transporter Tyt1, a novel neurotransmitter:sodium symporter from *Fusobacterium nucleatum*. *J. Biol. Chem.* **281,** 26444–26454 (2006).
11. Forrest, L. R. *et al.* Mechanism for alternating access in neurotransmitter transporters. *Proc. Natl Acad. Sci. USA* **105,** 10338–10343 (2008).
12. Kniazeff, J. *et al.* An intracellular interaction network regulates conformational transitions in the dopamine transporter. *J. Biol. Chem.* **283,** 17691–17701 (2008).
13. Noskov, S. Y. Molecular mechanism of substrate specificity in the bacterial neutral amino acid transporter LeuT. *Proteins* **73,** 851–861 (2008).
14. Noskov, S. Y. & Roux, B. Control of ion selectivity in LeuT: two Na^+ binding sites with two different mechanisms. *J. Mol. Biol.* **377,** 804–818 (2008).
15. Shi, L. *et al.* The mechanism of a neurotransmitter:sodium symporter — inward release of Na^+ and substrate is triggered by substrate in a second binding site. *Mol. Cell* **30,** 667–677 (2008).
16. Singh, S. K. LeuT: a prokaryotic stepping stone on the way to a eukaryotic neurotransmitter transporter structure. *Channels (Austin)* **2,** 380–389 (2008).
17. Crisman, T. J., Qu, S., Kanner, B. I. & Forrest, L. R. Inward-facing conformation of glutamate transporters as revealed by their inverted-topology structural repeats. *Proc. Natl Acad. Sci. USA* **106,** 20752–20757 (2009).
18. Khalili-Araghi, F. *et al.* Molecular dynamics simulations of membrane channels and transporters. *Curr. Opin. Struct. Biol.* **19,** 128–137 (2009).
19. Li, J. & Tajkhorshid, E. Ion-releasing state of a secondary membrane transporter. *Biophys. J.* **97,** L29–L31 (2009).
20. Quick, M. *et al.* Binding of an octylglucoside detergent molecule in the second substrate (S2) site of LeuT establishes an inhibitor-bound conformation. *Proc. Natl Acad. Sci. USA* **106,** 5563–5568 (2009).
21. Shi, L. & Weinstein, H. Conformational rearrangements to the intracellular open states of the LeuT and ApcT transporters are modulated by common mechanisms. *Biophys. J.* **99,** L103–L105 (2010).
22. Zhao, Y. *et al.* Single-molecule dynamics of gating in a neurotransmitter transporter homologue. *Nature* **465,** 188–193 (2010).
23. Singh, S. K., Piscitelli, C. L., Yamashita, A. & Gouaux, E. A competitive inhibitor traps LeuT in an open-to-out conformation. *Science* **322,** 1655–1661 (2008).
24. Claxton, D. P. *et al.* Ion/substrate-dependent conformational dynamics of a bacterial homolog of neurotransmitter:sodium symporters. *Nature Struct. Mol. Biol.* **17,** 822–829 (2010).
25. Singh, S. K., Yamashita, A. & Gouaux, E. Antidepressant binding site in a bacterial homologue of neurotransmitter transporters. *Nature* **448,** 952–956 (2007).
26. Beckett, D., Kovaleva, E. & Schatz, P. J. A minimal peptide substrate in biotin holoenzyme synthetase-catalyzed biotinylation. *Protein Sci.* **8,** 921–929 (1999).
27. Zhou, Z. *et al.* LeuT-desipramine structure reveals how antidepressants block neurotransmitter reuptake. *Science* **317,** 1390–1393 (2007).
28. Zhou, Z. *et al.* Antidepressant specificity of serotonin transporter suggested by three LeuT-SSRI structures. *Nature Struct. Mol. Biol.* **16,** 652–657 (2009).
29. Sen, N., Shi, L., Beuming, T., Weinstein, H. & Javitch, J. A. A pincer-like configuration of TM2 in the human dopamine transporter is responsible for indirect effects on cocaine binding. *Neuropharmacology* **49,** 780–790 (2005).
30. Piscitelli, C. L., Krishnamurthy, H. & Gouaux, E. Neurotransmitter/sodium symporter orthologue LeuT has a single high-affinity substrate site. *Nature* **468,** 1129–1132 (2010).

Supplementary Information is linked to the online version of the paper at www.nature.com/nature.

Acknowledgements We thank R. Altman for assistance in preparing reagents for single-molecule experiments and F. Carvalho for the preparation of membranes. Molecular graphics were prepared with PyMOL. Computations were performed on Ranger at the Texas Advanced Computing Center (TG-MCB090022) and the David A. Cofrin computational infrastructure of the Institute for Computational Biomedicine at Weill Cornell Medical College. This work was supported in part by National Institutes of Health grants DA17293 and DA022413 (J.A.J.), DA12408 (H.W.), DA023694 (L.S.), the Irma T. Hirschl/Monique Weill-Caulier trusts (S.C.B.) and the Lieber Center for Schizophrenia Research and Treatment. D.S.T. is supported by the Tri-Institutional Training Program in Computational Biology and Medicine.

Author Contributions Y.Z. expressed, purified and labelled the LeuT mutants. M.Q. and Y.Z. performed the functional characterization of the mutants. Y.Z. and D.S.T. designed, carried out and analysed the single-molecule experiments; L.S. and H.W. designed and analysed the computational studies, which were carried out by L.S.; S.C.B. and J.A.J. helped to design the biochemical and single-molecule experiments and, with L.S. and H.W., helped to interpret the data. All the authors contributed to writing and editing the manuscript.

Author Information Reprints and permissions information is available at www.nature.com/reprints. The authors declare no competing financial interests. Readers are welcome to comment on the online version of this article at www.nature.com/nature. Correspondence and requests for materials should be addressed to J.A.J. (jaj2@columbia.edu) or S.C.B (scb2005@med.cornell.edu).

METHODS

Protein expression and purification. LeuT variants were expressed in *E. coli* C41(DE3) as described[15]. For functional studies, LeuT variants were expressed from pQO18 or derivatives thereof carrying the indicated mutations[20], whereas for single-molecule FRET studies, biotin acceptor peptide-tagged LeuT variants were expressed in pETO18G and its derivatives[22]. Protein was purified by immobilized metal (Ni^{2+}) affinity chromatography using a Ni^{2+} Sepharose 6 FastFlow column (GE Healthcare)[22]. For fluorescent labelling of LeuT, Cy3-maleimide and Cy5-maleimide (GE Healthcare) were added at an equimolar ratio (200 μM total) for 1 h while the protein was bound to the Ni^{2+} resin[22]. Free dye was removed before the elution of LeuT with 300 mM imidazole.

Scintillation proximity-based binding studies. Binding of ^{3}H-leucine or ^{3}H-alanine (146 Ci mmol^{-1} and 49.4 Ci mmol^{-1}, respectively; both from Moravek) to purified LeuT-variants was measured with the scintillation proximity assay (SPA) as described[15], with 25 ng of purified protein per assay in buffer composed of 150 mM Tris/MES, pH 7.5/50 mM NaCl/1 mM TCEP/0.1% n-dodecyl-β-D-maltopyranoside or 50 mM Tris/MES, pH 7.5/150 mM LiCl/1 mM TCEP/0.1% n-dodecyl-β-D-maltopyranoside. To determine the molar ratio of Leu (or Ala)-to LeuT, binding samples were incubated with increasing concentrations of radioligand and measured in the SPA c.p.m. mode of the Wallac 1450 MicroBeta counter (Perkin Elmer). The efficiency of detection was calculated with standard curves of known concentrations of ^{3}H-Leu or ^{3}H-Ala. The standard curves were used to transform c.p.m. into the amount of bound substrate[15]. The amount of LeuT in the SPA assays was determined[31]. SPA-based binding studies using 2 μM [^{22}Na]Cl (1,017 mCi mg^{-1}; Perkin Elmer) were performed in 150–200 mM Tris/MES, pH 7.5/1 mM TCEP/0.1% n-dodecyl-β-D-maltopyranoside in the presence of 0–50 mM NaCl (equimolar replacement of Tris/MES to maintain a total molarity of 200 mM)[15]. All experiments were repeated at least in duplicate with triplicate determination of all individual data points. Kinetic constants (shown ± the s.e.m. of the fit) were obtained by fitting the data from independent experiments to global fitting in Prism or SigmaPlot.

^{3}H-Ala transport in proteoliposomes. Proteoliposomes were prepared as described[15]. The accumulation of ^{3}H-Ala (49.4 Ci mmol^{-1}; Moravek) was measured at 23 °C in assay buffer composed of 150/50 mM Tris/MES (pH 8.5) and 50 mM NaCl/150 mM LiCl. The reaction was quenched by the addition of ice-cold assay buffer without radiotracer and the proteoliposomes were collected on GF-75 glass fibre filters (Advantec) before the determination of the accumulated c.p.m. by liquid scintillation counting.

Single-molecule FRET imaging experiments. Fluorescence experiments were performed using a prism-based total internal reflection fluorescence (TIRF) microscope as previously described[22,32]. Microfluidic imaging chambers were passivated with a mixture of PEG and biotin-PEG and incubated with 0.8 μM streptavidin (Invitrogen). Cy3/Cy5-labelled, biotinylated LeuT molecules were surface immobilized through biotin-streptavidin interaction. Cy3 fluorophores were excited by the evanescent wave generated by total internal reflection (TIR) of a single-frequency light source (Ventus 532, Laser Quanta). Photons emitted from Cy3 and Cy5 were collected using a 1.2 NA 60× water-immersion objective (Nikon) and optical treatments were used to separate Cy3 and Cy5 frequencies onto a cooled, back-thinned EMCCD camera (Cascade 512, Photometrics). Fluorescence data were acquired using Metamorph (Universal Imaging Corporation).

All experiments were performed in buffer containing 50 mM Tris/MES, pH 7.5, 10% glycerol, 0.02% (w/v) DDM, 5 mM 2-mercaptoethanol and 200 mM salt (KCl or NaCl, as specified). We used an oxygen-scavenging environment (1 unit per ml glucose oxidase, 8 units per ml catalase, 0.1% (v/v) glucose) containing 2 mM cyclooctatetraene in all experiments to minimize photobleaching.

Analysis of single-molecule fluorescence data was performed using custom software written in MATLAB (MathWorks). A subset of the acquired traces was selected for further analysis using the following criteria: (1) single-step donor photobleaching, (2) signal-to-background noise ratio (SNR) ≥ 8, (3) <4 donor blinking events, (4) non-zero FRET efficiency for at least 60 s. Additional manual trace selection was performed to refine the data, where selected traces were required to have: (1) stable total fluorescence intensity ($I_D + I_A$) and (2) at least one transition between clearly defined FRET states with anti-correlated transitions in donor/acceptor intensity or a single dwell in a clearly-defined FRET state. We found this process to be effective in removing artefacts and spurious noise without introducing significant bias (see Supplementary Discussion and Supplementary Fig. 10).

Kinetic analysis was performed to idealize FRET traces and calculate average dwell times using a three-state model as previously described[22]. Error bars for transition rate estimates and FRET histograms were calculated as the standard deviation of 100 bootstrap samples of the traces. Error bars for state occupancies were calculated from 1,000 bootstrap samples.

Transition rates were interpreted using transition state theory, where the open and closed states are considered ground states separated by a large ($\Delta G^{\ddagger} \approx 80$ kJ mol^{-1}) activation barrier (the transition state). The energy required to achieve the transition state (and cross the barrier) was calculated as:

$$\Delta G^{\ddagger} = -RT \ln\left(\frac{hk_{i,j}}{k_B T}\right),$$

where R is the gas constant, T is absolute temperature (296 K), h is Planck's constant, k is the measured transition rate, from state i to state j, and k_B is Boltzmann's constant. Changes in the activation barrier energy ($\Delta\Delta G^{\ddagger}$) were calculated from the difference in forward and reverse rates observed in the absence and presence of substrate.

Molecular dynamics. The Li^+-only simulation was performed on a system prepared as described[24]. Briefly, it consisted of more than 77,000 atoms, including the explicit membrane model, solvating water molecules and the various ions and ligands. All the Na^+ ions in the system were replaced with Li^+. The parameters for Li^+ were from ref. 33. All MD simulations were carried out with the NAMD program under constant temperature (310 K) and constant pressure (1 atm) conditions. Long equilibration runs were performed to allow the system to transition to a new stable conformation. The inward-closed and inward-open conformations described in Supplementary Fig. 9 were based on the simulations described previously[22]. More than one MD trajectory was collected for every configuration studied. Each individual trajectory was at least 360 ns, and the longest trajectory for each configuration was 720 ns. All the results reinforced the conclusions, and the structural and dynamic insights described in the main text were revealed as the common features and trends of parallel independent MD runs.

31. Schaffner, W. & Weissmann, C. A rapid, sensitive, and specific method for the determination of protein in dilute solution. *Anal. Biochem.* **56,** 502–514 (1973).
32. Munro, J. B., Altman, R. B., O'Connor, N. & Blanchard, S. C. Identification of two distinct hybrid state intermediates on the ribosome. *Mol. Cell* **25,** 505–517 (2007).
33. Caplan, D. A., Subbotina, J. O. & Noskov, S. Y. Molecular mechanism of ion-ion and ion-substrate coupling in the Na^+-dependent leucine transporter LeuT. *Biophys. J.* **95,** 4613–4621 (2008).

doi:10.1038/nature09971

Supplementary Discussion

Comparative simulation analysis of the bound Li^+ vs. Na^+ in the LeuT structure. Monitoring long molecular dynamics (MD) simulations performed with either Na^+ or Li^+ in the established Na^+ binding sites and in the absence of substrate, we identified differences in the conformational changes occurring in this region of LeuT in the presence of Li^+ compared to those observed in the presence of Na^+ (Ref 1) (**Fig. 3b-c**).

In the Na1 site, Li^+ maintained interactions with T254 and E290, as was also observed for Na^+; however, Li^+ appeared less stably bound, and the connections bridging TM1 and TM6 were lost, so that neighboring packing interactions were affected. In particular, the configurations of residues F252 and F253 in the conserved aromatic cluster at the extracellular side of the S1 binding site were rearranged, and these differences were propagated to the interaction between the F252-F253-F259 triad in TM6, and the G408-T409/V412-V413 stretches in TM10. Thus, in the Li^+-only simulation, the backbone of G408 adopts a partially flipped configuration and the side chains of residues T409 and V413 adopt alternative rotamer states compared to the Na^+-only simulation (**Fig. 3b-c**; **Supplementary Fig. 8**). These changes produce a modestly distorted helical turn in TM10 in this key region of the extracellular vestibule, close to the residues of the S2 site along this TM, i.e., L400 and D404. Together, differences in the configuration of G408-T409 and V412-V413 in TM10 observed in comparing the Li^+-bound to the Na^+-bound forms of the transporter appear to propagate ion-specific effects that involve the cluster of aromatic residues at the heart of the S1 binding site (**Fig. 3b-c, Supplementary Fig. 8**).

The extracellular portion of TM10 forms the S2 site together with residues from TM1, TM3, and EL4[1]. The propagation of ion-specific conformational changes we found to be centered around TM10 contributes to the allosteric transmission of the impact of substrate binding in the S2 site, through the Na1 and S1 sites, to the intracellular end of the transporter molecule (**Supplementary Fig. 9**). This proposed allosteric pathway consists of the following main steps: *i*) the bound S2 substrate acts on TM10 directly through its interactions with L400 and D404, *ii*) the S2-residues I111, L400, and D404 are in close associations with Y107 and Y108, which participate in the configurational changes of the F252-F253-F259 triad in TM6, the relevance of which to the Na1 site is

discussed above. The result is a rearrangement of the interface between TM6 and TM10. We find that in terms of the coordination of direct ion binding and propagating the ion-specific effects, the dynamics at the TM6/TM10 interface is symmetrical in its relation to the Na1 site, to that of the TM1/TM5 interface in its relation to the Na2 site[2]. We also note that the set of residues found to participate in the signal propagation pathway along TM10 correspond to residues that were shown in mutational studies of the cognate serotonin transporter (SERT) to affect functional and allosteric properties in a manner consistent with the present findings. For example, cysteine substitutions of T503 or E508, which correspond to F414 and E419 in LeuT[3], and the mutation of the SERT TM10 sequence A505 to I507, which corresponds in LeuT to G416 to T418, disrupted the effects of allosteric modulators in SERT[4,5].

Photophysical transitions to zero-FRET. As previously described[6], significant fluctuations toward zero-FRET are observed within open-state dwells. As the frequency of these transitions is dependent on the laser illumination intensity (data not shown), we interpret these transitions as photophysical blinking events, where the acceptor fluorophore briefly transitions into a non-flourescent dark state.

Evaluating potential bias in trace selection. To make robust kinetic analysis feasible with the data obtained, in which a significant fraction of molecules imaged exhibited low signal-to-noise ratios, manual trace selection methods were used to examine specifically the subset of traces (~30%), where such artifacts were lacking and distinct FRET states were clearly evident.

To examine any potential bias from this process, FRET histograms were generated from each dataset before and after trace selection (**Supplementary Fig. 10**). Manual trace selection, while modestly altering the width of each FRET state observed, did not meaningfully alter the information content of the data, as evidenced by the observation that: 1) the relative occupancies of the two FRET states observed were largely unchanged; and 2) the FRET distributions for both the unfiltered and filtered datasets respond similarly to addition of ligands. Such results are consistent with the selected data being representative of the ensemble.

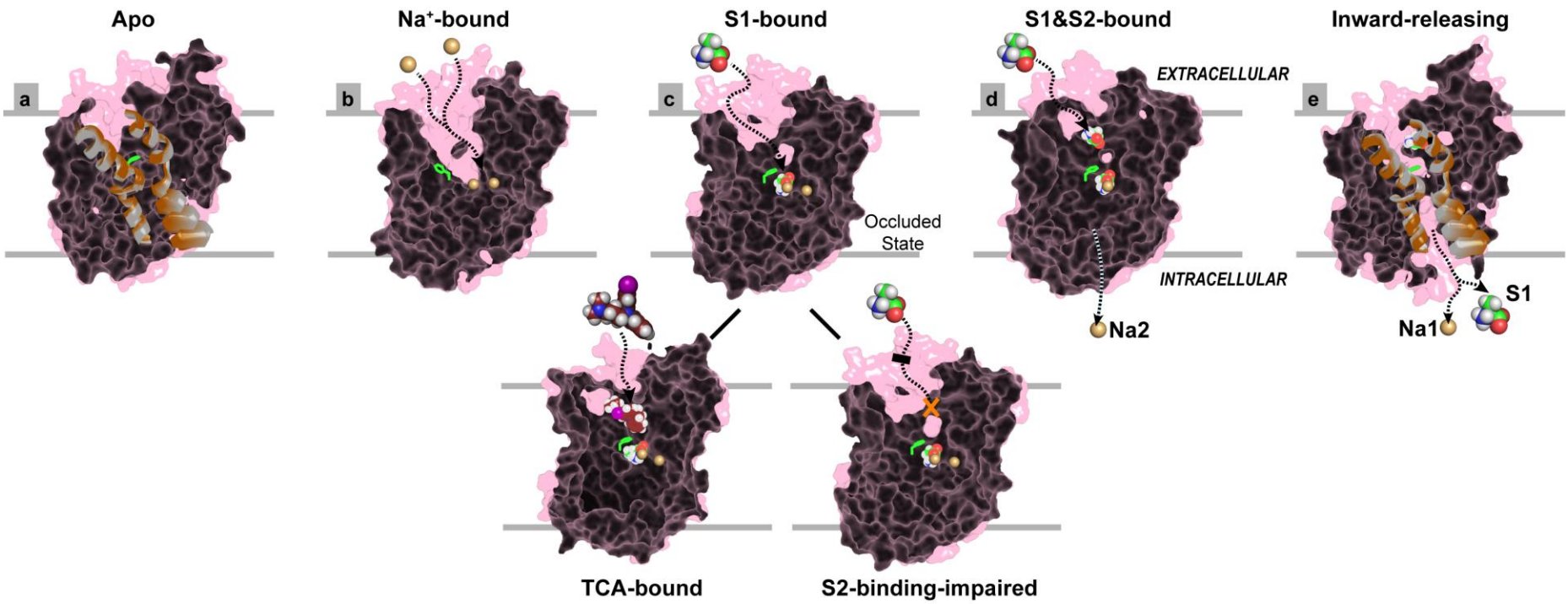

Supplementary Figure 1. Scheme showing components of the transport cycle for which experimental, computational, and in some cases crystallographic data are available. These include **a**) apo, **b**) Na^+-bound, **c**) S1-bound, TCA-bound, S2-binding impaired, **d**) S1 & S2-bound, and **e**) inward-releasing conformations[7]. Note that intracellular gate dynamics monitored with the dyes positioned at H7C and R86C do not necessarily detect all the conformational changes at the intracellular end of the transporter. To emphasize the dynamic changes, TM1 and TM6 are shown in panels (**a**) and (**e**) in ribbon representations of the space swept in the simulation between their positions in the closed and open conformations: The inward-releasing conformation identified in the inward-pulling SMD and subsequent MD is shown in gray in (**a**) and orange in (**e**), and the intermediate positions are shown by morphing from the inward-closed conformation to the inward-open to illustrate the relevant dynamics. The binding and unbinding of Na^+, the substrate Ala, or the TCA, CMI, are shown by dotted lines with arrowheads. The S2 site mutant shown has a greatly reduced affinity for Ala in the S2 site and is therefore S2-binding impaired as indicated by the black bar. In all panels, Phe253 in TM6, which after a rotamer switch participates in forming a cap over the S1 site, is shown in green.

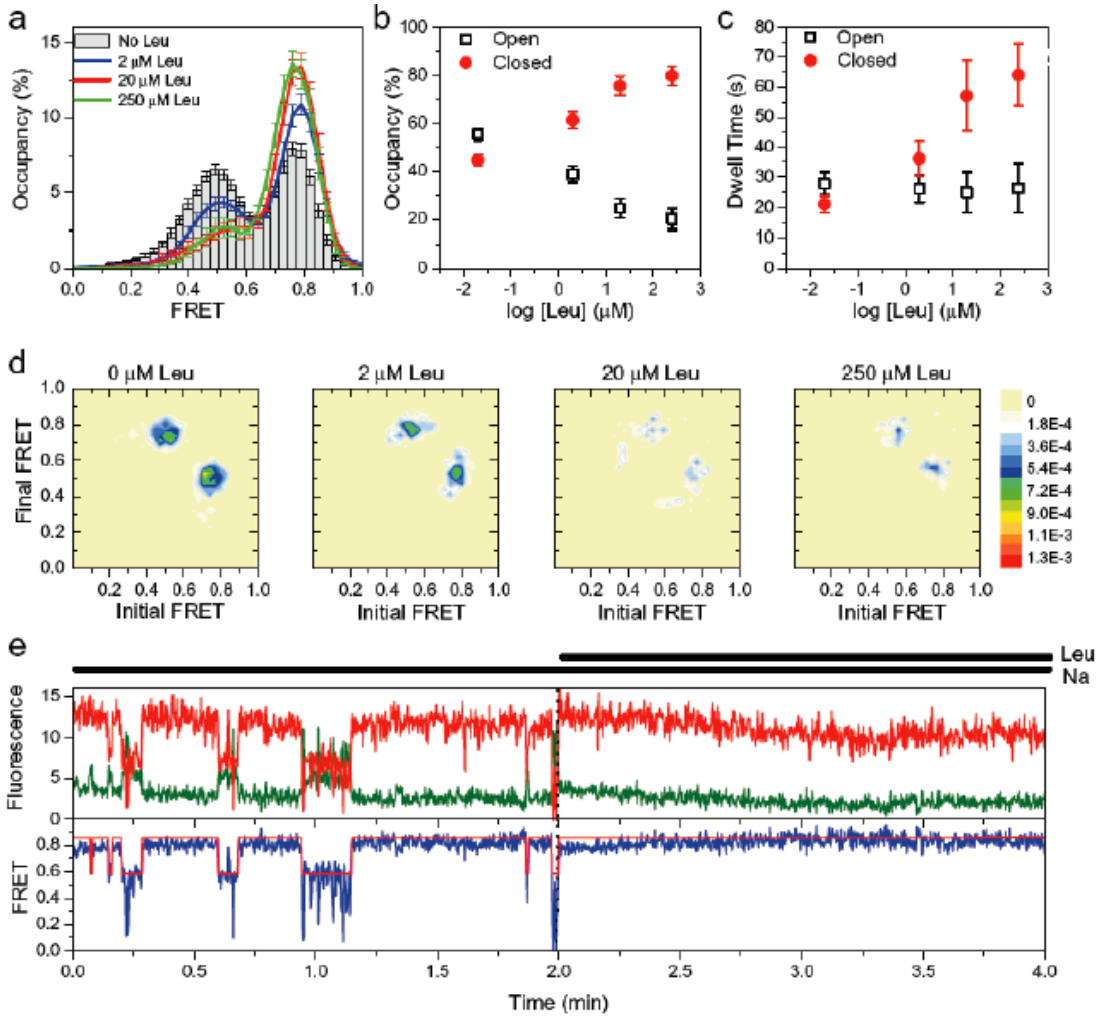

Supplementary Figure 2: Effect of leucine on LeuT dynamics. smFRET imaging of surface-immobilized Cy3/Cy5-labeled H7C/R86C-LeuT was performed at 160 ms time resolution in buffer containing 2 mM NaCl and various concentrations of L-leucine (Leu). (**a**) The FRET data (at least 90 selected traces per condition) were filtered to remove fluorophore dark states (see **Methods**) and summed into a histogram to compare occupancy in specific FRET states. (**b**) The FRET traces were idealized with a two state model. The fraction of time spent in the lower-FRET open state (black open squares) and the high-FRET closed state (red closed circles) was calculated from the idealization. (**c**) Average dwell times in the open state (black open squares) and the closed state (red filled circles) were estimated using maximum likelihood fitting. (**d**) Transition density plots were created by plotting the average FRET value before (x-axis) and after (y-axis) each transition between distinct FRET states. Transitions to dark states were computationally removed for clarity. (**e**) A representative single-molecule trajectory is

shown from an experiment where imaging started in 2 mM Na^+ followed by solution exchange to 2 mM Na^+ and 250 μM Leu at the 2-minute time point.

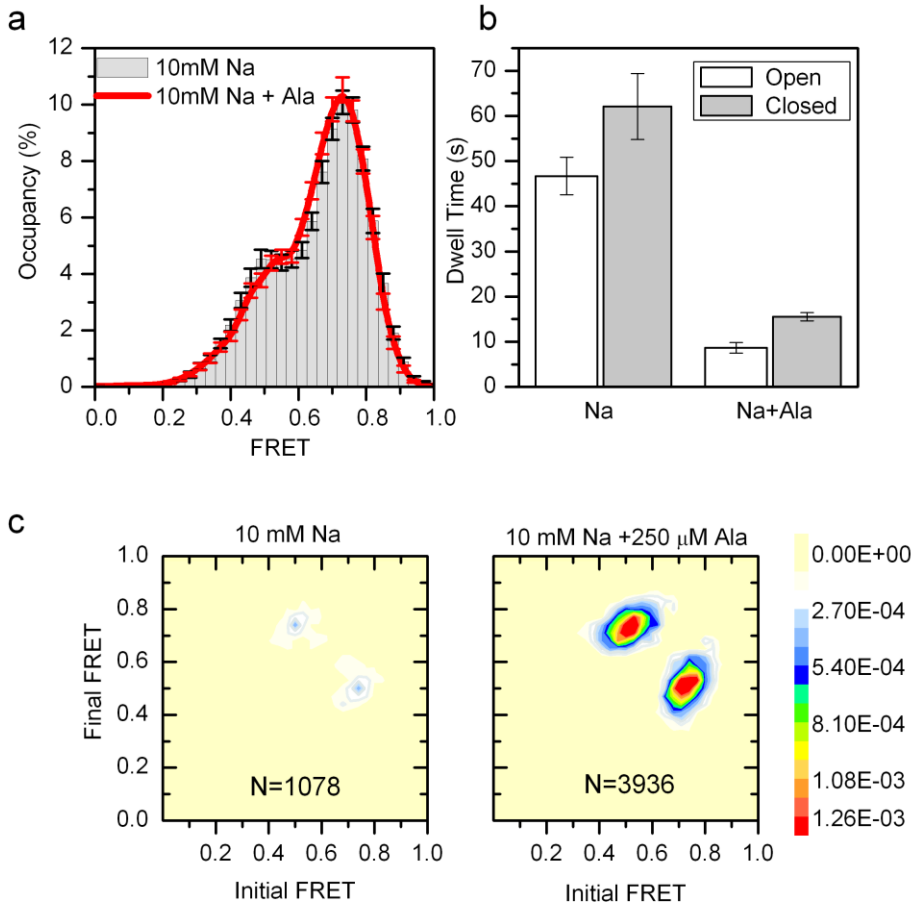

Supplementary Figure 3: smFRET imaging of surface-immobilized Cy3/Cy5-labeled H7C/T515C-LeuT performed in buffer containing 10 mM NaCl or 10 mM NaCl plus 250 μM alanine. (**a**) The FRET data (at least 380 selected traces per condition) were filtered to remove fluorophore dark states (see **Methods** and **Supplementary Discussion**) and summed into a histogram to compare the occupancies of specific FRET states. Error bars are the standard deviation of 1000 bootstrap samples. (**b**) Maximum likelihood analysis was performed on the idealizations to estimate the average lifetime of the open (white) and closed (gray) states. Error bars are the standard deviation of 100 bootstrap samples. (**c**) Transition density plots generated for each condition.

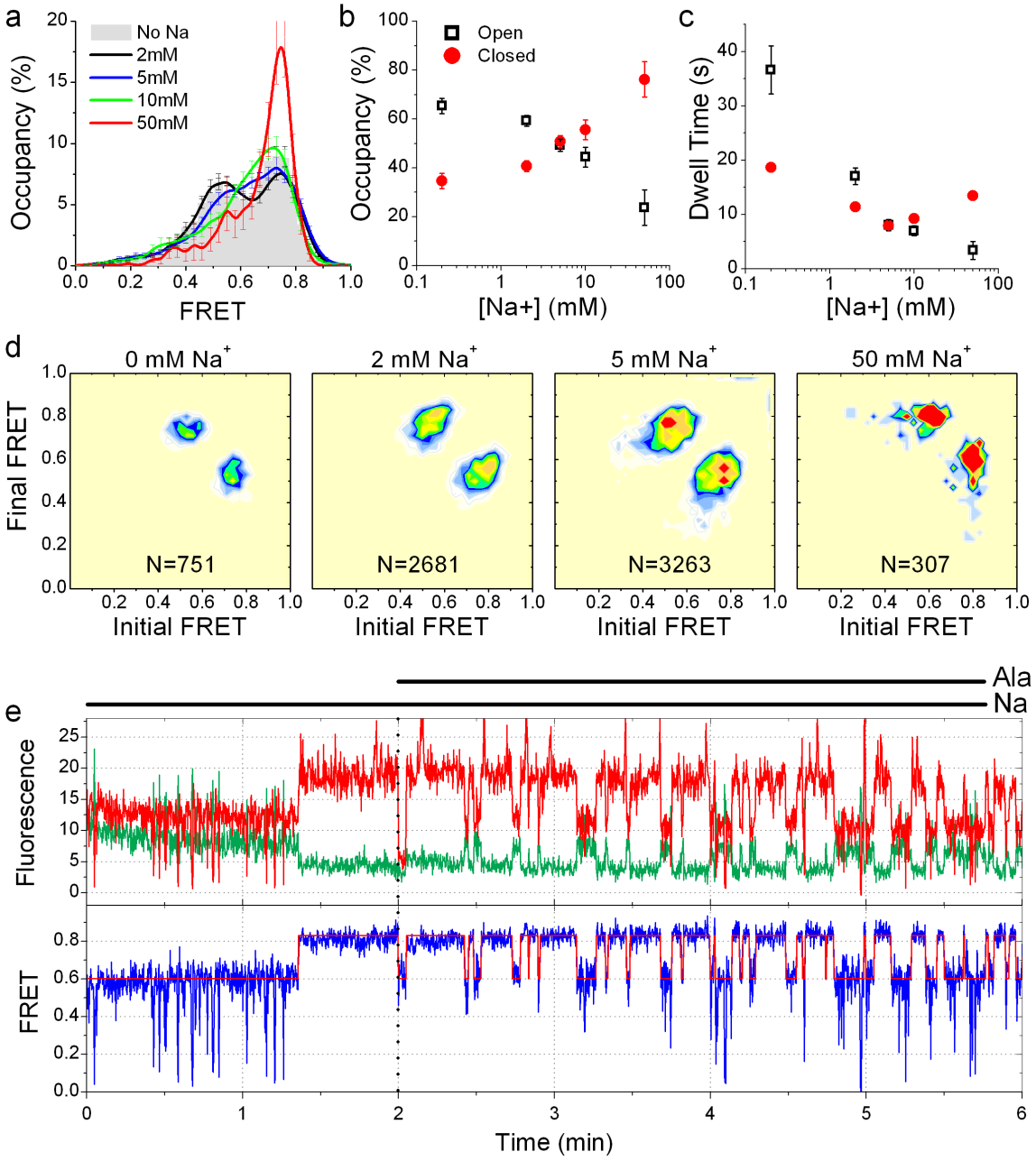

Supplementary Figure 4: smFRET imaging of surface-immobilized Cy3/Cy5-labeled H7C/R86C-LeuT was performed in buffer containing 250 μM alanine over a range of NaCl concentrations. (**a**) The FRET data were filtered to remove fluorophore dark states (see **Methods**) and summed into a histogram to compare occupancy in specific FRET states. (**b**) FRET traces were idealized using a two-state, hidden Markov model and the fraction of time spent in the low-FRET (open black squares) and high-FRET (filled red circles) states is shown. Error bars are the standard deviation of 1000 bootstrap samples. (**c**) Maximum likelihood analysis was performed on the idealizations to estimate the

average lifetime of the open (open black squares) and closed (red filled circles) states. Error bars are the standard deviation of 100 bootstrap samples. (**d**) Transition density plots of each condition, (**e**) A representative single-molecule trajectory is shown (Cy3 donor intensity in green, Cy5 acceptor intensity in red, FRET in blue and idealization in red), where the experimental conditions started in 0 mM NaCl and 2 mM Ala, followed by exchange to 2 mM NaCl and 2 mM Ala at the 2-minute time point.

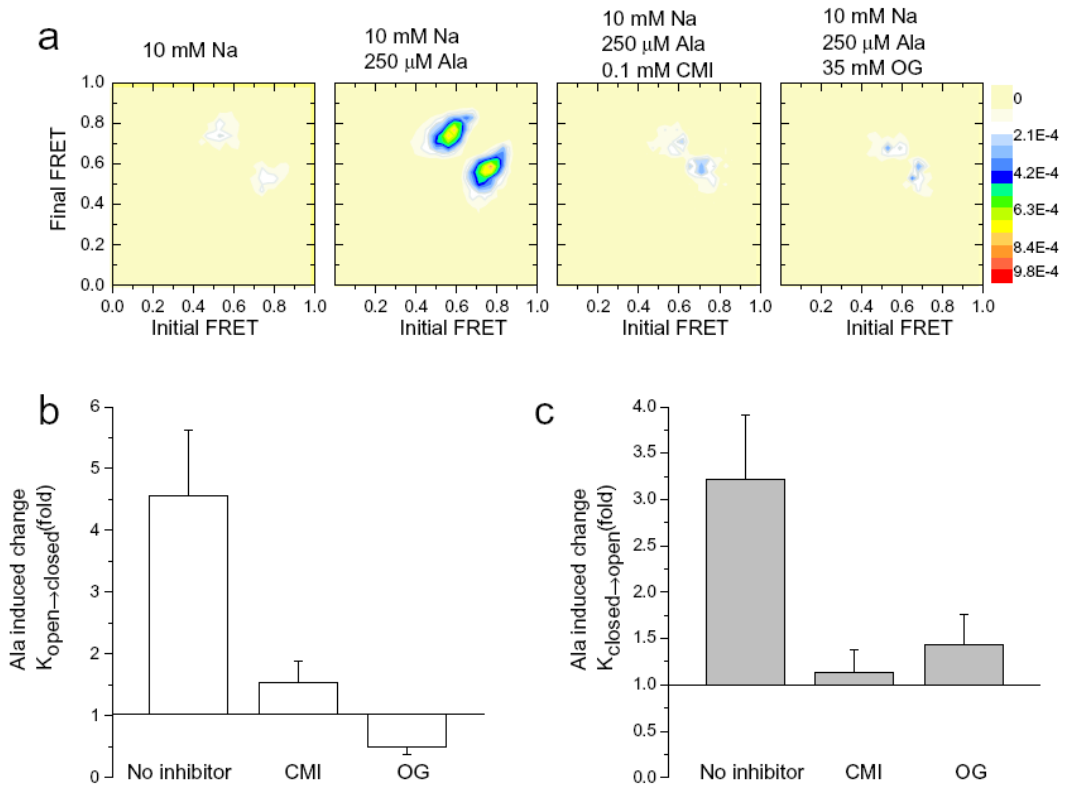

Supplementary Figure 5: Effect of transport inhibitors on LeuT dynamics. (**a**) Transition density plots were created by plotting the average FRET value before (x-axis) and after (y-axis) each transition between distinct FRET states. (**b-c**) The fold change (relative to the 10 mM Na^+ condition) in the rate of transitioning from the open state to the closed state (open bars, **b**) and from the closed state to the open state (filled bars, **c**) is shown for Cy3/Cy5-labeled H7C/R86C-LeuT in 10 mM Na^+ plus 250 μM Ala alone (no inhibitor) or with an additional 0.1 mM CMI, or 35 mM OG (from at least 100 selected traces per condition).

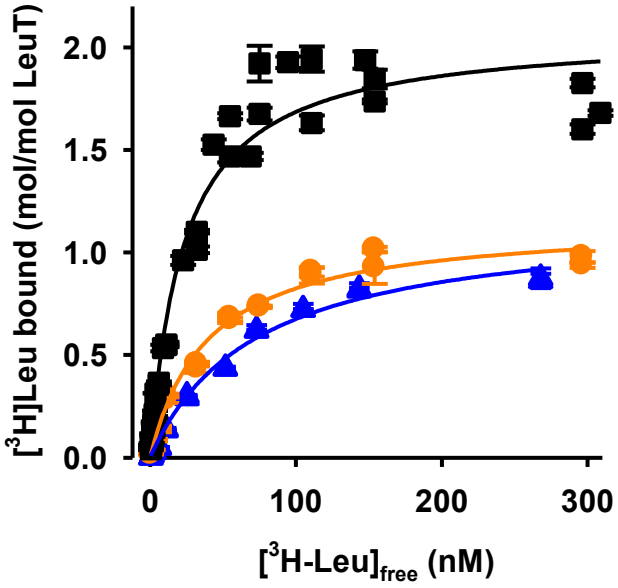

Supplementary Figure 6: Saturation binding of ^{3}H-Leu. The stoichiometry of ^{3}H-Leu binding by WT-LeuT (■), L400S (●), and F253A (▲) was assayed with 25 ng protein in the presence of increasing concentrations of ^{3}H-Leu (146 Ci/mmol) in 50 mM NaCl-containing assay buffer with the scintillation proximity assay[7]. Data of independent experiments (n≥2) were subjected to one-site binding global fitting yielding the following Leu-to-LeuT stoichiometries and EC_{50}s: WT-LeuT: 2.08 ± 0.07, 23.3 ± 3.1 nM; L400S: 1.15 ± 0.04, 39.8 ± 3.9 nM; F253A: 0.93 ± 0.056, 73.1 ± 10.9 nM (mean ± SEM of the fit).

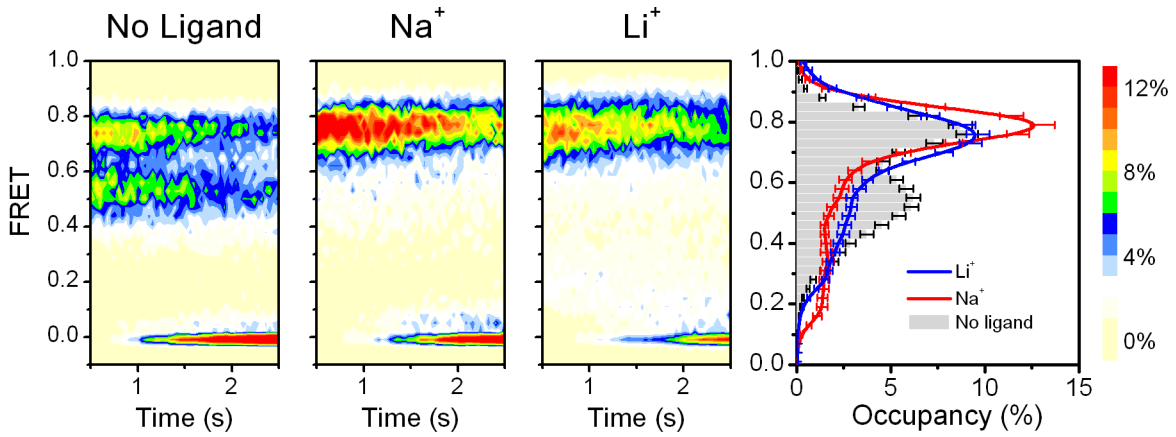

Supplementary Figure 7: smFRET imaging of surface-immobilized Cy3/Cy5-labeled H7C/R86C-LeuT performed in buffer containing 200 mM KCl (left panel), NaCl (center left panel), or LiCl (center right panel) and summed into population histograms (right panel). For each condition the mean value and relative occupancies of each FRET state were estimated by summing the data into one-dimensional histograms, where dark states were computationally filtered (see **Methods**): 200 mM KCl. (gray bars); 200 mM NaCl (red line); and 200 mM LiCl (blue line). All datasets contain at least 290 selected traces.

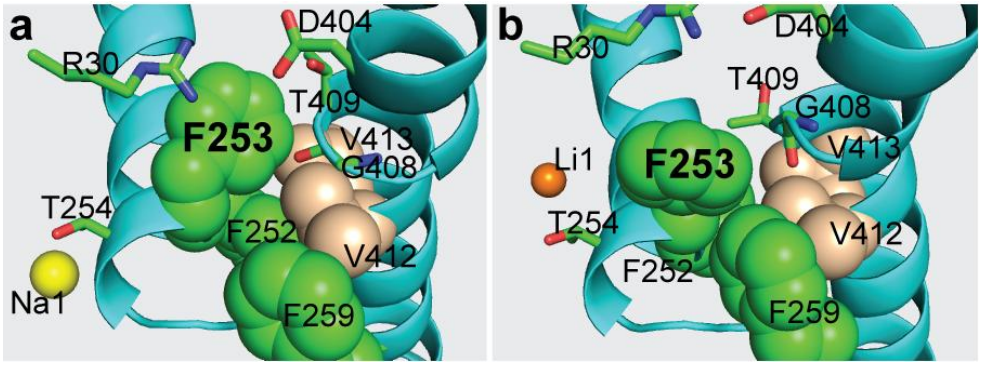

Supplementary Figure 8. Zoom-in views of the different effects of Na^+ (**a**) and Li^+ (**b**) on the close associations of the aromatic cluster in TM6 and residues in TM10. See also **Fig. 3** in the main text.

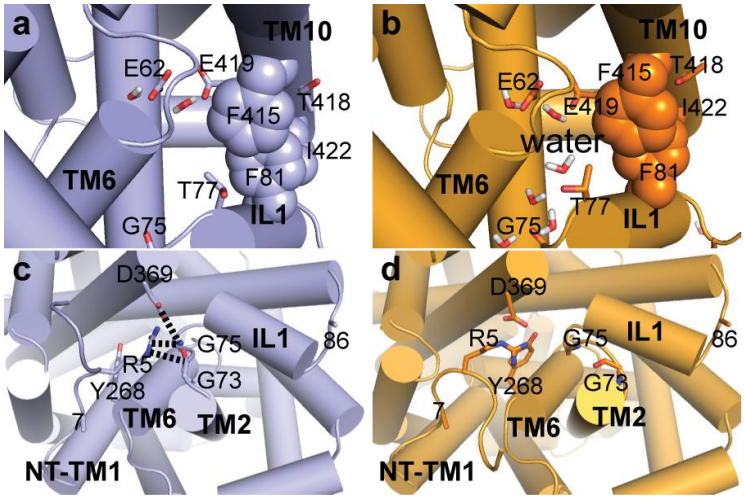

Supplementary Figure 9. Representation of the changes occurring at the intracellular end of LeuT as a result of inward-pulling SMD followed by MD equilibration. Conformational changes of residues at the interface of TMs 6 and 10 in the inward-closed state (panels **a**,**c**, shown in blue) are propagated towards the intracellular end of LeuT and trigger the transition to an inward-open state (panels **b**,**d**, shown in orange). Comparison of panels **a** and **b** shows the increase in water penetration facilitated by the propagation of these conformational changes from the extracellular sides of TMs 6 and 10, through the junction of TM6, TM10, and IL1 that is held together by E419 (TM10) and E62 (TM2) at the unwound region of TM6. The junction is opened by the rearrangement of interactions between IL1 and TM10, i.e., between T77 and F81 (IL1) and three TM10-residues: F415, T418, and I422. The result of the opening of this junction is evidenced by the comparison of panels **c** and **d**: The interactions between IL1 (G73 and G75) and the conserved salt-bridge-cation:π network (R5-D369-Y268) (shown in **c**) is disrupted as shown in (**d**). Together, these changes eventually lead to rearrangements in the NT-TM1 region, including the movement of TM1a registered by the change in distance between positions 7 and 86 as described and discussed previously[6] and read out by the smFRET experiments.

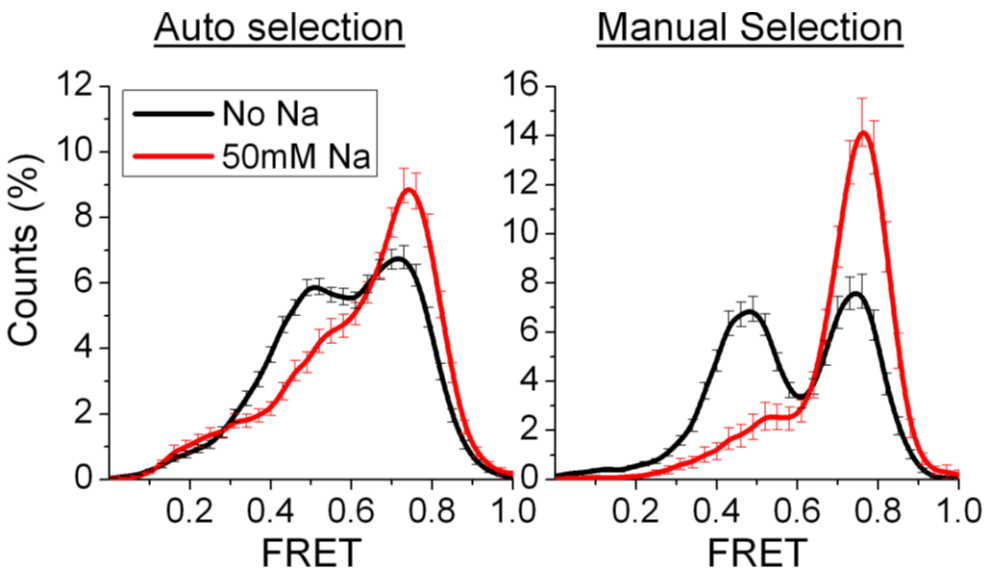

Supplementary Figure 10. For kinetic analysis of smFRET traces from dye-labeled LeuT, manual trace selection methods were used to examine specifically the subset of traces where distinct FRET states were clearly evident and to filter out traces with low signal-to-noise ratios (see **Methods** and **Supplementary Discussion**). To examine whether the selection process introduces bias in the analysis, we compared FRET histograms generated from traces automatically selected (N>350, left panel) to those selected manually (right panel, N>90) under two conditions: no Na^+ or substrate (black lines) and 50 mM Na^+ and no substrate (red lines). This analysis demonstrated that although some changes in the widths of the FRET distributions are observed as a result of trace selection: 1) similar relative occupancies of the two states are apparent in each condition; and 2) with the addition of Na^+, changes observed in the FRET distribution are similar. These results are consistent with the selected subset of data being representative of the ensemble.

	EC_{50} (mM Na^+)	cpm_{max}	n_H
WT	8.9 ± 0.7	99460 ± 5688	2.03 ± 0.3
H7C/R86C	8.6 ± 0.3	96430 ± 2107	2.24 ± 0.2
H7C/R86C-Cy3,Cy5	8.3 ± 0.6	92970 ± 3587	2.19 ± 0.38
L400S	9.9 ± 0.6	94150 ± 3471	2.07 ± 0.27
F253A	7.9 ± 0.9	94050 ± 5795	2.22 ± 0.6

Supplementary Table 1: Na^+ binding kinetics of WT-LeuT and indicated LeuT-variants. Binding of 2 µM $^{22}NaCl$ was determined at concentrations of non-radioactive NaCl from 0 – 50 mM by means of the scintillation proximity assay[7]. Maximum $^{22}Na^+$ binding in the absence of unlabeled NaCl is shown as counts per minute (cpm_{max}). Data were fitted to the Hill equation to obtain EC_{50} (corresponding to the concentration of NaCl at 50% cpm_{max}) and the Hill coefficient (n_H). Kinetic constants are expressed as the mean ± SEM (n = 6) of the fit.

Supplementary References

1 Claxton, D. P. et al., Ion/substrate-dependent conformational dynamics of a bacterial homolog of neurotransmitter:sodium symporters. *Nat Struct Mol Biol* **17** (7), 822 (2010).

2 Shi, L. and Weinstein, H., Conformational rearrangements to the intracellular open states of the LeuT and ApcT transporters are modulated by common mechanisms. *Biophys J* **99** (12), L103.

3 Keller, P. C., 2nd, Stephan, M., Glomska, H., and Rudnick, G., Cysteine-scanning mutagenesis of the fifth external loop of serotonin transporter. *Biochemistry* **43** (26), 8510 (2004).

4 Zhong, H. et al., An allosteric binding site at the human serotonin transporter mediates the inhibition of escitalopram by *R*-citalopram: kinetic binding studies with the ALI/VFL-SI/TT mutant. *Neurosci Lett* **462** (3), 207 (2009).

5 Neubauer, H. A., Hansen, C. G., and Wiborg, O., Dissection of an allosteric mechanism on the serotonin transporter: a cross-species study. *Mol Pharmacol* **69** (4), 1242 (2006).

6 Zhao, Y. et al., Single-molecule dynamics of gating in a neurotransmitter transporter homologue. *Nature* **465** (7295), 188 (2010).

7 Shi, L. et al., The mechanism of a neurotransmitter:sodium symporter - inward release of Na^+ and substrate is triggered by substrate in a second binding site. *Mol Cell* **30** (6), 667 (2008).